
Article:
Dixon Wilkins, M.C. orcid.org/0000-0003-1520-7672, Stennett, M.C., Maddrell, E. et al. (1 more author) (2020) The formation of stoichiometric uranium brannerite (UTi2O6) glass-ceramic composites from the component oxides in a one-pot synthesis. Journal of Nuclear Materials, 542. 152516. ISSN 0022-3115

https://doi.org/10.1016/j.jnucmat.2020.152516

Journal of Nuclear Materials 542 (2020) 152516

Contents lists available at ScienceDirect

Journal of Nuclear Materials

journal homepage: www.elsevier.com/locate/jnucmat

The formation of stoichiometric uranium brannerite (UTi_2O_6) glass-ceramic composites from the component oxides in a one-pot synthesis

Malin C. Dixon Wilkins[a,*], Martin C. Stennett[a], Ewan Maddrell[b], Neil C. Hyatt[a]

[a] Department of Materials Science and Engineering, University of Sheffield, UK
[b] National Nuclear Laboratory, Sellafield, Cumbria, UK

ARTICLE INFO

Article history:
Received 13 July 2020
Revised 1 September 2020
Accepted 6 September 2020
Available online 11 September 2020

Keywords:
Glass-ceramics
Radioactive wasteforms
Brannerite
Uranium compounds

ABSTRACT

Brannerite glass-ceramic composites have been suggested as suitable wasteform materials for high-actinide content wastes, but the formation of glass-ceramic composites containing stoichiometric uranium brannerite (UTi_2O_6) has not been well-studied. Uranium brannerite glass-ceramic composites were synthesised at by a one-pot cold-press and sinter route from the component oxides. As a comparison, two further samples were produced using an alkoxide-nitrate route. A range of compositions with varying molar ratios of uranium and titanium oxides (from 1:2 to 1:3.20) were synthesised, with a range of different heat treatments (1200 °C for 12–48 h, and 1250 °C for 12 h). All compositions were analysed by X-ray diffraction, scanning electron microscopy, energy dispersive X-ray spectroscopy, and X-ray near-edge spectroscopy, and found to contain UTi_2O_6 as the majority crystalline phase forming within a glass matrix of nominal stoichiometry $Na_2AlBSi_6O_{16}$. In compositions with UO_2:TiO_2 ratios of 1:2 and 1:2.28, particles of UO_2 were observed in the glass matrix, likely due to dissolution of TiO_2 in the glass phase; this was prevented by the addition of excess TiO_2. This work demonstrates the suitability of this system to produce highly durable wasteforms with excellent actinide waste loading, even with a simple one-pot process. Some grains of brannerite consist of a UO_2 particle encapsulated in a shell of UTi_2O_6, suggesting that brannerite crystallises around particles of UO_2 until either the UO_2 is fully depleted, or the kinetic barrier becomes too large for further diffusion to occur. We propose that the formation of brannerite within glass-ceramic composites at lower temperatures than that for pure ceramic brannerite is caused by an increase in the rate of diffusion of the reactants within the glass.

1. Introduction

Alongside glass and ceramic materials, glass-ceramic composites are one of the promising candidates for immobilisation of high activity radioactive wastes [1–4]. They have attracted particular attention for use as flexible host matrices for high actinide content wastes that are otherwise unfit for reprocessing [5–7]. A suitable glass-ceramic composite has the benefit of high actinide waste loading due to the ability of ceramics to contain much higher actinide contents than glasses, but still retain the chemical flexibility of glasses, able to contain and immobilise contaminant and/or fission product species [8].

Brannerite (UTi_2O_6) has been proposed as a suitable target ceramic phase in glass-ceramics due to the retention of the brannerite structure even when doped with extremely high proportions of actinide elements (stoichiometric UTi_2O_6 has a uranium content of > 55% by weight) [9,10]. It crystallises in the monoclinic space group *C*2/*m* (No. 12), with a structure consisting of sheets of staggered, edge- and corner-sharing (TiO_6) octahedra (similar to TiO_2 anatase), with adjacent sheets connected by chains of corner-sharing (UO_6) octahedra [11,12]. Examples of natural brannerites (with the oldest being found in host rocks 1.58 billion years old, and the youngest between 5 and 11 million years old) [13,14] are generally found to have been amorphised over time by their high actinide content (metamictisation), but still retain a large proportion of their original uranium inventory, with A-site uranium atoms per formula unit of 0.4 to 0.9 [15,16]. It is also of interest that natural brannerites have been found to contain a wide range of dopant cations (including Ca, Pb, Th, Y, and REE on the

* Corresponding author.
E-mail address: mdixonwilkins1@sheffield.ac.uk (M.C. Dixon Wilkins).

https://doi.org/10.1016/j.jnucmat.2020.152516

U site, and Fe, Al, and Si on the Ti site [15–17]), as the introduction of lower valent cations (commonly Gd^{3+}, Ca^{2+}, or Y^{3+}) has been found to have a strong effect on the formation of the brannerite structure under oxidising conditions by charge balancing higher valent U^{5+} and U^{6+} cations [9, 18–20]. If brannerite is to be considered as a wasteform for disposal of damaged or degraded MOX fuels, then this flexibility with regards to cation content allows for introduction of neutron absorbers such as Hf and/or Gd to address criticality concerns. In this respect, it is notable that Turuani et al., recently reported a comprehensive investigation of lanthanide abundance in brannerites, which was shown to reflect the geological conditions of formation [16].

The direct synthesis of ceramic UTi_2O_6 from the component oxides is hampered by slow diffusion through the solid state. This can be simply remedied by increasing the reaction temperature (*e.g.* reacting at 1400 °C rather than 1300 °C), increasing the reaction time, or by introducing an intermediate re-grinding of the sample to break up reacted material, re-exposing the reactants. Other synthetic routes reported in the literature use wet chemical processes to ensure mixing of the reactants occurs at the nano- or atomic-scale, followed by a reaction at high temperature. The most commonly reported method is an alkoxide-nitrate route, utilising U-nitrate and Ti-isopropoxide (this is discussed in more detail below), but other methods using soluble U and/or Ti precursors have been reported. Mesbah et al. reported a comparison of four different synthetic routes, including a dry oxide-based route, the alkoxide-nitrate route, an acetate-sulphate route, and a hydroxide route starting from U-chloride and Ti-isopropoxide [21].

Although brannerite glass-ceramic composite materials have been reported in the literature, only a single study has attempted the production of end-member U-, Th-, and Ce-brannerite glass-ceramic composites. In that study, we observed that UTi_2O_6 (and to a lesser extent $ThTi_2O_6$) crystallises well in the $Na_2AlBSi_6O_{16}$ glass system, assuming that atmospheric pO_2 is conducive to an average composition with overall 4+ charge on the A-site. Glass-ceramic composites with UTi_2O_6 as the ceramic phase have not yet been extensively studied, but are of interest as a model system for understanding structure – composition – property relationships. The majority of brannerite phases reported as crystallising in glass have been U^{5+} species, with M^{3+} doped onto the U-site to act as a charge balancer (including trivalent Y, Eu, Tb, Dy and mixed tri- and tetravalent Ce) [22–25]. All previous uranium brannerite glass-ceramics introduced the ceramic phase as a ceramic precursor prepared by calcining a stir-dried alkoxide-nitrate reaction mixture at 700 °C under either air or Ar (for Pu-containing samples). The ceramic precursor was then mixed with a glass precursor, pressed into pellets, and heat treated at 1200 °C. For the purpose of industrial application, it would be useful to develop a one-pot synthetic route for brannerite glass-ceramics, from the component oxides and a glass precursor, reducing the number of handling operations necessary to produce the final wasteform. The development of such a synthesis route, applied to stoichiometric UTi_2O_6 brannerite glass-ceramics, is the focus of this contribution. It is envisaged that, in a conceptual industrial process, wasteforms would be produced by hot isostatic pressing (HIP). This means that the wasteform material would ideally form at or below 1300 °C (the maximum service temperature for stainless steel HIP canisters), to avoid necessitating the use of more expensive and exotic alloys. This presents a challenge to the formation of pure or doped ceramic UTi_2O_6 by solid state reaction, which generally requires temperature in excess of 1300 °C (typically in the range of 1320–1350 °C).

2. Experimental

Brannerite glass-ceramic compositions were prepared by a one-pot cold-press and sinter method. The glass phase (composition $Na_2AlBSi_6O_{16}$) was introduced as a batched precursor, prepared by calcining a stoichiometric mixture of H_3BO_3, Na_2CO_3, Al_2O_3 and SiO_2 at 600 °C for 6 h. The ceramic components were added as the oxides, UO_2 and TiO_2 (anatase).

A stoichiometric mixture of UO_2 and TiO_2 (as UO_2 was observed in compositions with required amounts of UO_2 and TiO_2 (excess TiO_2 was added to form some compositions (see Table 1)), were milled together with the precursor mixture in a Fritsch Pulverisette 23 reciprocating ball mill for 5 min at 30 Hz. The resulting slurry was dried in an oven at 85 °C and the powder retrieved and broken up using a mortar and pestle. The milled powders were pressed into 10 mm diameter pellets under 2 t (approx. 250 MPa). The green pellets were placed into crucibles on a bed of coarse ZrO_2 to prevent attachment to the crucible surface, then heat treated in a tube furnace under an inert (Ar) atmosphere. Any ZrO_2 adhered to the outside of the pellets was manually removed.

The heat-treated pellets were broken into pieces for characterisation. Powder X-ray diffraction (XRD) was used to identify the phases present (Bruker D2 Phaser using Ni-filtered Cu Kα radiation), and the relative quantities of the crystalline phases were qualitatively measured using a standard Rietveld refinement method, utilising the software package TOPAS [26,27]. For the purpose of crystalline phase quantification, the amorphous content was neglected, as it contributed little to the overall diffraction pattern in the presence of UTi_2O_6 and UO_2. The background was modelled with a tenth order shifted Chebyshev polynomial and peak shapes were modelled using Pseudo-Voigt functions. The unit cell parameters of each phase (UTi_2O_6 and UO_2, with TiO_2 in some compositions) were allowed to refine, along with the atomic positions of U and Ti. XRD is insensitive to light elements such as O, especially in the presence of heavy elements such as U, so the atomic positions of O were not refined.

Scanning Electron Microscopy with coupled Energy Dispersive X-ray analysis (SEM-EDX) was used to examine the microstructure and microchemical composition of the glass-ceramic products (Hi-

Table 1
As-batched oxide stoichiometries (samples U9 and U10 were produced following an alkoxide-nitrate synthesis) and details of heat treatments for different UTi_2O_6 glass-ceramics. The difference in each composition relative to a parent composition is underlined (*i.e.* U5 to U8 had the same starting composition as U3, but underwent different heat treatments).

ID	Glass	UO_2	TiO_2	U:Ti molar ratio	Heat treatment
U1	50.00%	31.42%	18.58%	1:2	1200 °C, 12 h, Ar
U2	48.75%	30.63%	20.62%	1:2.28	1200 °C, 12 h, Ar
U3	47.50%	29.85%	22.65%	1:2.57	1200 °C, 12 h, Ar
U4	45.00%	28.28%	26.71%	1:3.20	1200 °C, 12 h, Ar
U5	47.50%	29.85%	22.65%	1:2.57	1200 °C, 24 h, Ar
U6	47.50%	29.85%	22.65%	1:2.57	1200 °C, 36 h, Ar
U7	47.50%	29.85%	22.65%	1:2.57	1200 °C, 48 h, Ar
U8	47.50%	29.85%	22.65%	1:2.57	1250 °C, 12 h, Ar
U9	50.00%	31.42%	18.58%	1:2	1200 °C, 12 h, H_2/N_2
U10	47.50%	29.85%	22.65%	1:2.57	1200 °C, 12 h, H_2/N_2

tachi TM3030, operating at 15 kV; Bruker Quantax 70 EDX system). Samples were prepared for SEM-EDX by mounting in a cold set epoxy resin, before polishing to an optical finish using increasingly finer grades of abrasive paper and diamond suspensions (finishing at 1 μm) and coating with a conductive carbon layer.

The alkoxide-nitrate synthesis is described in detail elsewhere [22]. The reaction mixture was calcined for 24 h at 700 °C under a reducing atmosphere (5% H_2 in N_2). The calcine was then used in place of UO_2 and TiO_2 to form a glass-ceramic following the cold-press and sinter method detailed above. Two compositions were made by this route: U9, with a U:Ti ratio of 1:2, and U10, with a U:Ti ratio of 1:2.57, matching other compositions in this study prepared by a one-pot cold press and sinter process, as well as similar titanate ceramics and glass-ceramics in the literature (many contain a small excess of Ti-isopropoxide to encourage full reaction of the mixture and to account for loss of isopropoxide as it readily hydrolyses in air and disperses).

In order to confirm the uranium oxidation state, X-ray absorption spectra were acquired in fluorescence mode at Diamond Light Source beamline B18 [28]. Diamond Light Source operates with an electron energy of 3 GeV and a beam current of 300 mA. Samples were prepared by mixing a small amount of the materials to be examined with polyethylene glycol and pressing into pellets. Spectra were collected at room temperature and pressure in the range 16,940 to 17,970 eV, with a step size of 0.3 eV, and a counting time of 200 ms per step. The energy was selected using a Si (111) monochromator, and aligned using the K-edge of an yttrium metal foil. A 36 element Ge solid state fluorescence detector was used. The data were processed and the resulting spectra analysed using the Demeter suite of programs [29].

The sample composition and heat treatments are summarised in Table 1. Of note is that additional TiO_2 was added by reducing both the targeted amount of UTi_2O_6 and glass (*e.g.* a sample with 10% additional TiO_2 can be described as a ratio of 45:45:10 glass:UTi_2O_6:TiO_2), this means that the overall weight percent of glass varies slightly between samples, from 45% to 50% (see Table 1 for further details). Previous work on glass-ceramic composites in this system has shown that the formation of UTi_2O_6 in the $Na_2AlBSi_6O_{16}$ system is relatively insensitive to the overall glass fraction, so this slight variation in glass fraction will not have a significant effect on the phase assemblages of each product [30].

3. Results

3.1. X-ray diffraction

All samples produced formed brannerite as the majority ceramic phase, with small amounts of UO_2 observed in the XRD patterns of all compositions except U8, and TiO_2 observed in those compositions made from component oxides having a target UO_2:TiO_2 ratio of 2.28 or greater (all compositions, other than U1, U2, and the alkoxide-nitrate samples U9 and U10). The results of qualitative phase abundances, as-derived from Rietveld refinements of XRD data, are shown in Table 2. Due to the presence of high molar fractions of uranium (a very strong scatterer of X-rays), the comparatively weakly scattering glass phase has a very low contribution to the overall diffraction pattern, so cannot be reliably quantified from XRD-based methods; however, qualitative observations can still be made from the trends observed. The values in Table 2 were calculated by using Rietveld refinements to obtain the relative abundances of the different crystalline phases present, then, with the assumption that all ceramic-forming precursors were accounted for in these phase abundances, reduced to the abundance present in the final glass-ceramic product, according to the as-batched weight fractions of glass and ceramic. In reality both UO_2 and TiO_2 were observed in the glass matrix, as well as in the crystalline phases, but for the purpose of identifying the trends observed in these samples, this is not a significant consideration. The as-refined unit cell parameters are in good agreement with reference values, with no significant changes caused by the differing synthetic conditions (see Supplementary Information Table 1). Some variation is seen, most obviously in the unit cell volumes, but, as the measurements did not include an internal standard, and the variation is small, we cannot confidently establish the variation to be attributable to differences in composition or synthesis.

When visually comparing the observed relative intensity of TiO_2 reflections in the series U1 to U4 (where all four samples underwent the same heat treatment, but had differing UO_2:TiO_2 molar ratios, from 1:2 in U1 to 1:3.20 in U4), it is clear that addition of hyperstoichiometric amounts of TiO_2 does not lead to elimination of UO_2; indeed, TiO_2 is observed in samples U3 (approx. 2.22 wt%) and U4 (approx. 9.22 wt%).

Similarly, the phase assemblage of compositions with the same UO_2:TiO_2 ratio heat-treated at 1200 °C, but for differing lengths of time (samples U3, and U5–7), are very similar. As the length of heat treatment was increased from 12 to 48 h, the relative abundance of UO_2 reduces slightly (from approx. 1.10 wt% in U3 to 0.64 wt% in U7), and a corresponding reduction in the relative intensity of the UO_2 (111) reflection is also seen, but does not completely disappear. Similarly, when comparing a sample heat-treated at a higher temperature (U8, fired for 12 h at 1250 °C), to one with the same UO_2:TiO_2 ratio heat-treated at a lower temperature (U3, fired for 12 h at 1200 C), there is a marked reduction in the observed intensity of the UO_2 (111) reflection (however, UO_2 is observed in SEM micrographs, see Section 3.2). These observations

Table 2
Compositional information for samples U1-10. The glass composition was measured using EDX, averaging 10 regions of glass for each composition (B_2O_3 content was assumed to be as-batched), then converted into oxide wt%. The relative amounts of the crystalline phases as-determined from Rietveld refinements of XRD data are also shown.

ID	EDX glass composition (wt%)						Refinement of crystalline phase abundances (wt%)			U:Ti molar ratio
	SiO_2	Na_2O	Al_2O_3	B_2O_3	TiO_2	UO_2	UTi_2O_6	UO_2	TiO_2	
U1	73.3	9.6	6.8	2.5	5.5	2.4	48.41 ±0.09	1.60 ±0.09	–	1:2
U2	73.9	8.9	6.1	2.5	7.3	1.4	49.89 ±0.06	1.36 ±0.06	–	1:2.28
U3	71.8	10.6	6.0	2.5	7.6	1.5	49.18 ±0.30	1.10 ±0.06	2.22 ±0.31	1:2.57
U4	73.1	9.1	5.9	2.5	8.4	1.0	44.71 ±0.43	1.07 ±0.08	9.22 ±0.43	1:3.20
U5	68.4	10.8	6.0	2.5	8.5	3.9	45.68 ±0.34	0.23 ±0.08	6.58 ±0.34	1:2.57
U6	69.3	10.8	6.0	2.5	8.2	3.2	46.71 ±0.34	0.64 ±0.08	5.14 ±0.34	1:2.57
U7	72.2	9.5	5.9	2.5	6.6	3.3	45.83 ±0.56	0.60 ±0.15	6.07 ±0.55	1:2.57
U8	72.5	9.1	6.1	2.5	6.5	3.4	45.22 ±0.53	0.17 ±0.13	7.11 ±0.52	1:2.57
U9	72.3	8.8	6.0	2.5	9.0	1.5	44.93 ±0.10	5.07 ±0.10	–	1:2
U10	70.8	9.8	5.6	2.5	10.1	1.2	51.91 ±0.09	0.59 ±0.09	–	1:2.57

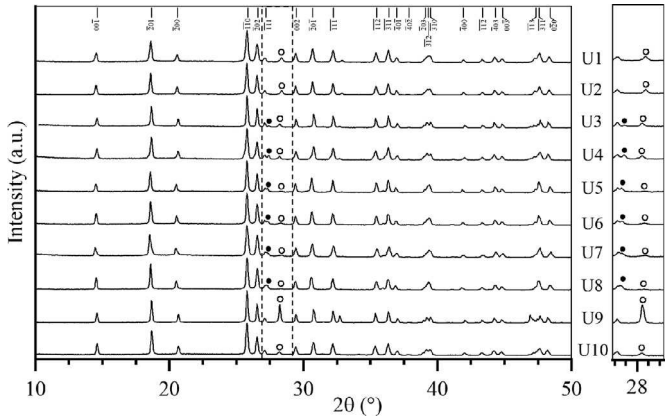

Fig. 1. XRD patterns of samples U1-U10 in the 2θ range 10–75° with a zoomed view (marked by the dashed border) of the 27–29° 2θ range. The reflections of UTi_2O_6 are marked with lines (PDF card 01-084-0496). The peaks associated with the TiO_2 (110) and UO_2 (111) reflections are marked with filled and empty circles respectively.

show that there is a relationship between heat treatment time and temperature, suggesting that diffusion kinetics play an important role in determining the phase assemblage.

The samples prepared by the alkoxide-nitrate route also formed brannerite as the major ceramic phase. U9 contains a relatively high amount of UO_2 (approx. 5.07 wt%, compared to $\leq$ 1.6 wt% for all other compositions) compared to other compositions, as judged from reflection intensity ratios (even sample U1 with the same target UO_2:TiO_2 ratio). The phase assemblage of U10 is very similar to that of U3, consisting of UTi_2O_6 as the majority phase, with a small amount of UO_2 also observed. This was expected from their compositions and similar conditions of heat treatment (the only difference being U10 was fired under a mixed H_2/N_2 atmosphere, whereas U3 was fired under Ar).

3.2. SEM-EDX

The phase assemblages observed by SEM were in good agreement with the XRD data previously discussed, and offer an explanation for the presence of residual UO_2 in all samples. A common feature in the microstructure of all samples was the presence of small regions of UO_2 within the interior of some brannerite ceramic grains; this suggests that brannerite forms around, and from, the original grains of UO_2. A plausible reaction mechanism would involve dissolution of TiO_2 in the glass phase, which then diffuses to, and reacts with, UO_2. The microstructures of all samples exhibited some macroscale porosity and smaller, irregular pores in large regions of glass. However, it was apparent that the ceramic phases did not exhibit any intragranular porosity. Examination of the microstructures of samples U1 and U9, batched with the lowest UO_2:TiO_2 molar ratio of 1:2, showed these compositions to have only partially reacted, with small clusters of UO_2 observed within the glass matrix throughout the samples, not just confined to the interior of brannerite grains. These particles of UO_2 are hereafter referred to as "free UO_2" to distinguish them from UO_2 observed within grains of brannerite. As the relative amount of TiO_2 with respect to UO_2 was increased from 1:2.28 to 1:3.20 in samples U2, U3, and U4 the inclusions of free UO_2 disappear, however, the incidence of UO_2 within the grains of brannerite remained effectively constant. Regions identified as TiO_2 were also observed in samples with other than U1 and U9, showing that at least some of the excess TiO_2 remains undissolved in the glass matrix (it is also possible that this TiO_2 had dissolved, but precipitated out of the glass as the materials cooled). Of note is that very small ($<$ 0.5 μm) regions of UO_2 are observed within grains of brannerite in sample U8 (see Fig. 2 for a comparison between samples U7 and U8), where it was not clearly apparent in the XRD pattern due to the relatively low sensitivity of XRD to phases with a particularly low concentration.

The samples heat treated for longer than 12 h show very similar microstructures, with no obvious differences from those heat treated for only 12 h. The grain sizes are approximately the same across U5, U6, and U7 (in the range 2 to 15 μm), suggesting that no significant growth of the brannerite grains in this glass system occurs on this timescale at the temperature used (1200 °C).

Although EDX is often a useful tool in analysing the elemental composition of materials such as these, the microstructure of these glass-ceramics make quantitative analysis difficult. As the volume of sample that characteristic X-rays are emitted from is larger than that of back-scattered electrons, the EDX spectrum may contain contributions from uranium and titanium dissolved within a region of glass and/or contributions from grain of brannerite located some distance below the surface of the region of glass. This leads to significant uncertainty in quantification of the EDX data, and must be taken into account when drawing conclusions from these analyses. This problem is compounded by the high molar fraction of light elements including oxygen and boron, as EDX is insensitive to such elements.

Quantification of EDX spectra of regions of glass in each sample largely yield the same result (B_2O_3 content was assumed to be equal to the as-batched content, see Table 2) - apparent uranium abundances (calculated assuming UO_2) in the glass are all $<$ 3.9 wt% with absolute errors of the magnitude ±0.3 wt%. It is apparent that the uranium content of the glass phase in all samples is very low, showing excellent partitioning of uranium into the ceramic phases. A spectrum of an area of sample U6 is shown in Fig. 3, and is representative of those seen in all samples. X-ray emission lines showing the presence of uranium and titanium are present but minor in comparison to those of glass-forming species.

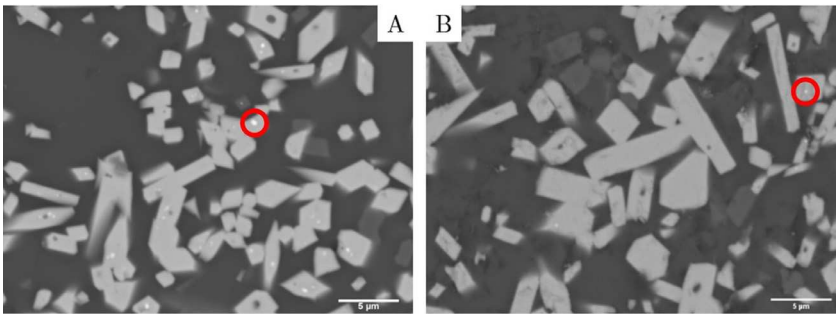

Fig. 2. Representative BSE micrographs of samples U7 and U8 (micrographs A and B respectively). White regions are UO_2, light grey are UTi_2O_6, dark grey are TiO_2, and the dark background is glass. Some regions of UO_2 are circled for clarity.

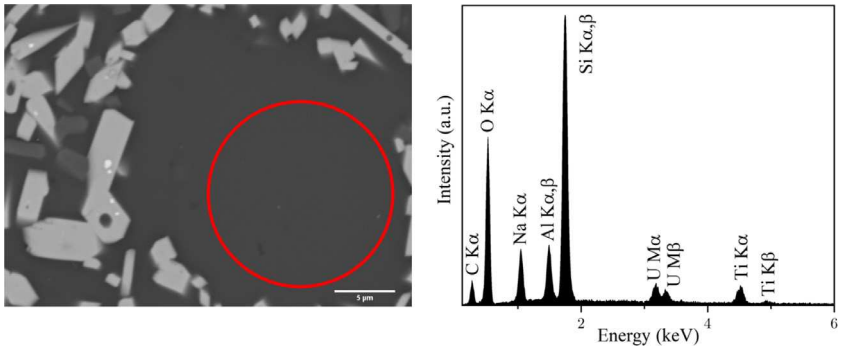

Fig. 3. BSE micrograph and associated EDX spectrum of U6. The region of glass relating to the spectrum is marked. The identities of each X-ray emission line are also marked. The presence of carbon is due to the conductive carbon coat applied during sample preparation.

It should be noted that these measurements will also contain possible systematic errors, and the results have only been used for qualitative analysis.

3.3. Uranium L_3-edge X-ray absorption near-edge spectroscopy

The average uranium oxidation states of all compositions, were examined using U L_3-edge XANES. The spectra of UTi_2O_6 and $U_{0.5}Yb_{0.5}Ti_2O_6$ were also acquired for use as reference compounds with known uranium oxidation state (U^{4+} and U^{5+} respectively). These reference compounds were chosen because they are both brannerite structured, giving them the closest possible match in uranium local structure, and so were the most relevant standards to measure in comparison to our samples. Samples of the ceramic precursors formed by the alkoxide-nitrate route were also analysed in order to confirm that the initial calcination under H_2/N_2 had fully reduced all of the U^{6+} starting material to U^{4+}. This is important, as all other brannerite glass-ceramics formed by an alkoxide-nitrate route were targeting U^{5+}, and so were calcined in either air or argon, with no control needed over the atmospheric pO_2.

The precise energy position of the U-L_3 X-ray absorption edge (the minimum energy necessary to remove a core electron) is dependent on the U oxidation state. Higher U oxidation states require more energy to remove an electron because each electron is more strongly bound to the nucleus, and *vice versa* for lower oxidation states. The E_0 values (as determined by the first maximum of the first derivative of intensity) of all compositions match that of the UTi_2O_6 standard, and the white line positions are also in excellent agreement (see Table 4). This showed that the uranium was present in all compositions as U^{4+}, as expected from the behaviour of ceramic brannerites in inert or reducing processing atmospheres such as those used in this study. It is promising that the precursors of U9 and U10 were fully reduced, even prior to the final heat treatment under a reducing atmosphere at 1200 °C, as it suggests that an inert atmosphere in this final step would be sufficient to retain the desired U^{4+} oxidation state.

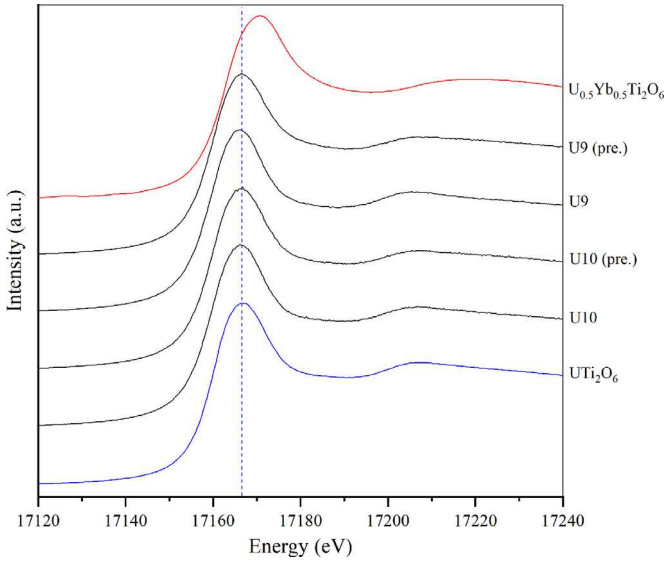

Fig. 4. Representative XANES spectra of samples U9, U10 and their ceramic precursors, along with those for UTi_2O_6 and $U_{0.5}Yb_{0.5}Ti_2O_6$ standards. The blue dashed line shows the white line energy position of the UTi_2O_6 standard.

Table 3
White line energy positions and E_0 (both in eV) values for all compositions U1-10, as well as the precursors to samples U9 and U10, and the standards of known valence UTi_2O_6 (4+) and $U_{0.5}Yb_{0.5}Ti_2O_6$ (5+), as determined from U L_3-edge XANES. E_0 was determined as the maximum in the first derivative of μ(X).

ID	White line position (eV)	E_0 (eV)
U1	17,167.1	17,161.1
U2	17,166.8	17,161.0
U3	17,166.6	17,161.1
U4	17,166.5	17,161.0
U5	17,167.1	17,161.2
U6	17,167.3	17,161.1
U7	17,167.1	17,161.0
U8	17,167.2	17,160.9
U9	17,166.6	17,161.0
U10	17,166.4	17,161.2
U9 (pre.)	17,166.6	17,161.0
U10 (pre.)	17,166.4	17,161.0
UTi_2O_6	17,166.7	17,161.1
$U_{0.5}Yb_{0.5}Ti_2O_6$	17,170.8	17,163.2

4. Discussion

With respect to the final glass-ceramic composite products, all compositions produced had favourable phase assemblages, with stoichiometric UTi_2O_6 being produced in every sample as the majority product, despite the processing temperature of 1200 °C remaining being below the 1300 °C usually necessary for full ceramic samples of UTi_2O_6 to form from their component oxides. It is thought that this increase in reactivity is caused by the presence of the glass phase increasing the ease of diffusion of the reactants, analogous to viscous phase assisted sintering. This is supported by the microstructures observed by SEM: regions of UO_2 held within grains of brannerite, as well as small amounts of both uranium and

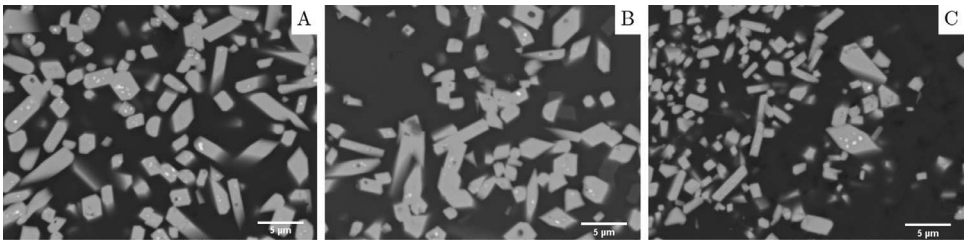

Fig. 5. Representative BSE micrographs of U2 (A), U7 (B), and U10 (C). Small white regions are UO_2, light grey are UTi_2O_6, dark grey are TiO_2, the dark background is glass.

titanium remaining dissolved in the glass matrix. The fact that all compositions formed large amounts of brannerite is important, as this demonstrates the ability of this system to form high-quality, high brannerite-fraction glass-ceramic composites using a simple one-pot cold-press and sinter method.

Sample U1 was the only composition produced from the component oxides where UO_2 particles are seen within the glass matrix (in addition to those regions of UO_2 seen in grains of brannerite), suggesting an incomplete reaction. There are two plausible reasons as to why some apparently unreacted UO_2 remains: either the amount of TiO_2 dissolved in the glass matrix was greater than that of UO_2 (this could be due to differences in solubility at high temperature, and/or solubility at low temperatures, resulting in precipitation), or the brannerite formed was actually U-deficient (resulting in excess UO_2, although synthetic uranium brannerites are not often reported to be non-stoichiometric, compared to cerium brannerites). As mentioned above, it is difficult to analyse how much uranium and titanium are dissolved in the glass using EDX, so this alone cannot distinguish the cause.

To address the presence of free UO_2 samples U2-4 were fabricated, with different amounts of excess TiO_2 added. The UO_2 (111) reflections seen in the diffraction patterns are less intense than that seen in U1, but there was only slight variation in intensity between U2, U3 and U4. This suggests that the addition of 2.5 wt% TiO_2 was sufficient to prevent formation of free UO_2 (and thus decrease the amount of UO_2 observed in the diffraction patterns), but not the UO_2 found within grains of brannerites. The observations from SEM support this interpretation, with no free UO_2 visible in U2, U3 or U4, but small regions of brannerite-encapsulated UO_2 seen in all three. In addition, grains of TiO_2 are also observed in increasing amounts. Further measurement and analysis of the uranium and titanium content in the glass phase will be investigated using more advanced synchrotron techniques; in particular, μ-focus X-ray fluorescence and μ-focus XANES measurements will allow for quantification of the uranium distribution and uranium oxidation states within the different phases of these samples.

The appearance of UO_2 encapsulated within grains of brannerite suggests that the reaction occurs at the surface of particles of UO_2, reaching a point, as the layer of brannerite grows, where diffusion becomes kinetically unfavourable. Samples U5-7 were heat treated for longer periods of time to see if an extended dwell at 1200 °C would be sufficient to allow full reaction of these UO_2 regions, however, the results do not fully bear this out; although there was a reduced amount of UO_2 observed, it was still present (if in trace amounts) in both the XRD and SEM. The same observations are extended to sample U8, where a higher reaction temperature of 1250 °C produced a product that only contained a very trace amount of UO_2. It is possible that this behaviour was caused either by an epitaxial mechanism of brannerite growth on the surface of particles of UO_2 or simply caused by the higher mobility of Ti^{4+} cations and/or particles of TiO_2 within the glass, leading to the reaction occurring closer to the particles of UO_2 (and eventually encapsulating them). It is clear that an important factor preventing a completely single-ceramic-phase product from forming was the kinetic barrier to diffusion caused by this encapsulation of the reactant UO_2.

The samples produced by an alkoxide-nitrate route (samples U9 and U10) display largely the same behaviour as the equivalent oxide stoichiometries. The notable difference being the relatively larger amount of UO_2 observed in the XRD pattern of U9. It is assumed this was caused by the ease at which titanium isopropoxide hydrolyses in air and is lost, leading to non-stoichiometry of the batch during processing. This was corrected for by the addition of excess titanium isopropoxide in sample U10, where the additional titanium precursor accounts for both this effect, and the amount of excess TiO_2 necessary to prevent formation of free UO_2. The phases observed by SEM agree with this interpretation (and match the trend seen in samples U1-4); where in sample U9 UO_2 was observed in the glass matrix and within grains of brannerite, whereas in sample U10 UO_2 was only rarely observed in grains of brannerite, comparable to the microstructure of sample U7. Of note is that the UTi_2O_6 grain sizes are of the same approximate magnitude as the samples made from solid state precursors, but tend to have a slightly wider range of grain sizes (see Fig. 5).

5. Conclusion

Near single-ceramic-phase UTi_2O_6 glass-ceramics were produced at 1200 and 1250 °C. The secondary crystalline phase present in all samples was UO_2, found held within grains of brannerite in all samples, as well as within the glass matrix in composition U1 and U9, both of which had the lowest UO_2:TiO_2 molar ratio of 1:2. The addition of excess TiO_2 prevented generation of UO_2 within the glass matrix, but small regions of UO_2 within grains of brannerite remained, even when samples were subjected to longer or higher temperature heat treatments (Figs. 1 and 4).

This microstructure leads to the observation that, whether caused by different rates of diffusion of the uranium and titanium species or by epitaxial growth of brannerite on the surface of UO_2 particles, the brannerite phase forms around regions of UO_2, until the thickness of the brannerite layer forms a kinetic barrier to diffusion and further reaction (resulting in regions of brannerite-encapsulated UO_2), or the core region of UO_2 is fully depleted (resulting in a grain of brannerite, with no observable UO_2 core).

The use of a ceramic precursor synthesised by an alkoxide-nitrate route did not have an effect on the phases formed. This is notable, as it confirms that a one-pot synthetic route allows or formation of high quality glass-ceramic products, without the additional heat treatment and handling steps necessary for an alkoxide-nitrate synthesis, or other wet chemical processes.

It is assumed that the presence of trace amounts of fully-encapsulated remnant UO_2 would not be an issue, but if materials similar to those produced in this study were to be suggested as a wasteform material for high U-content wastes, then the effect of the presence of this UO_2 would have to be examined to confirm they do not have a deleterious effect on final wasteform performance (Table 3).

Declaration of Competing Interest

The authors declare that they have no known competing financial interests or personal relationships that could have appeared to influence the work reported in this paper.

CRediT authorship contribution statement

Malin C. Dixon Wilkins: Investigation, Visualization, Writing - original draft, Writing - review & editing. **Martin C. Stennett:** Supervision, Writing - review & editing, Investigation. **Ewan Maddrell:** Supervision, Writing - review & editing. **Neil C. Hyatt:** Supervision, Conceptualization, Writing - review & editing, Project administration.

Acknowledgements

MDW is grateful to the UK EPSRC and Nuclear Decommissioning Authority for providing studentship through an EPSRC iCASE award. NCH is grateful to the Royal Academy of Engineering and the Nuclear Decommissioning Authority for funding. This research utilised the HADES/MIDAS facility and Henry Royce Institute at the University of Sheffield established with financial support from UKRI EPSRC and BEIS, under grant EP/T011424/1 and EP/P02470X/1 [31], and was supported in part by grant EP/S01019X/1.

Supplementary materials

Supplementary material associated with this article can be found, in the online version, at doi:10.1016/j.jnucmat.2020.152516.

References

[1] G.J. McCarthy, High-level waste ceramics: materials considerations, process simulation, and product characterization, Nucl. Technol. 32 (1) (Jan. 1977) 92–105, doi:10.13182/NT77-A31741.
[2] W.E. Lee, M.I. Ojovan, M.C. Stennett, N.C. Hyatt, Immobilisation of radioactive waste in glasses, glass composite materials and ceramics, Adv. Appl. Ceram. 105 (1) (Feb. 2006) 3–12, doi:10.1179/174367606X81669.
[3] R.C. Ewing, W.J. Weber, F.W. Clinard, Radiation effects in nuclear waste forms for high-level radioactive waste, Prog. Nucl. Energy 29 (2) (Jan. 1995) 63–127, doi:10.1016/0149-1970(94)00016-Y.
[4] R.C. Ewing, Nuclear waste forms for actinides, Proc. Natl. Acad. Sci. 96 (7) (Mar. 1999) 3432–3439, doi:10.1073/pnas.96.7.3432.
[5] M.L. Carter, H. Li, Y. Zhang, A.L. Gillen, E.R. Vance, HIPed tailored pyrochlore-rich glass-ceramic waste forms for the immobilization of nuclear waste, MRS Online Proc. Libr. Arch. 1124 (Jan. 2008), doi:10.1557/PROC-1124-Q04-01.
[6] E. Maddrell, S. Thornber, N.C. Hyatt, The influence of glass composition on crystalline phase stability in glass-ceramic wasteforms, J. Nucl. Mater. 456 (Jan. 2015) 461–466, doi:10.1016/j.jnucmat.2014.10.010.
[7] Y. Zhang, Z. Zhang, G. Thorogood, E.R. Vance, Pyrochlore based glass-ceramics for the immobilization of actinide-rich nuclear wastes: From concept to reality, J. Nucl. Mater. 432 (1) (Jan. 2013) 545–547, doi:10.1016/j.jnucmat.2012.08.035.
[8] E.R. Vance, M.L. Carter, G.R. Lumpkin, R.A. Day, and B.D. Begg, 'Solid Solubilities of Pu, U, Gd and Hf in Candidate Ceramic Nuclear Wasteforms', Australian Nuclear Science and Technology Organization, Menai, NSW 2234, Australia (US), DOE/ER/45676; Project Number 60387, Apr. 2001. doi: 10.2172/781161.
[9] M. James, M.L. Carter, J.N. Watson, The synthesis, crystal chemistry and structures of Y-doped brannerite (U1−xYxTi2O6) and thorutite (Th1−xYxTi2O6−δ) phases, J. Solid State Chem. 174 (2) (Sep. 2003) 329–333, doi:10.1016/S0022-4596(03)00230-5.
[10] Y. Zhang, D.J. Gregg, G.R. Lumpkin, B.D. Begg, M. Jovanovic, The incorporation of neptunium and plutonium in thorutite (ThTi2O6), J. Alloys Compd. 581 (Dec. 2013) 665–670 no. Supplement C, doi:10.1016/j.jallcom.2013.07.115.
[11] R. Ruh, A.D. Wadsley, The crystal structure of ThTi2O6 (brannerite), Acta Crystallogr. 21 (6) (Dec. 1966) 974–978, doi:10.1107/S0365110X66004274.
[12] J.T. Szymanski, J.D. Scott, A crystal-structure refinement of synthetic brannerite, UTi 2 O 6, and its bearing on rate of alkaline-carbonate leaching of brannerite in ore, Can. Mineral. 20 (2) (May 1982) 271–280.
[13] K.R. Ludwig, J.A. Cooper, Geochronology of Precambrian granites and associated U-Ti-Th mineralization, northern Olary province, South Australia, Contrib. Mineral. Petrol. 86 (3) (Jun. 1984) 298–308, doi:10.1007/BF00373676.
[14] D. Gasquet, et al., Miocene to Messinian deformation and hydrothermal activity in a pre-Alpine basement massif of the French western Alps: new U-Th-Pb and argon ages from the Lauziere massif, Bull. Soc. Geol. Fr. 181 (3) (May 2010) 227–241, doi:10.2113/gssgfbull.181.3.227.
[15] G.R. Lumpkin, S.H.F. Leung, J. Ferenczy, Chemistry, microstructure, and alpha decay damage of natural brannerite, Chem. Geol. 291 (Jan. 2012) 55–68 no. Supplement C, doi:10.1016/j.chemgeo.2011.09.008.
[16] M. Turuani, et al., Geochemical fingerprints of brannerite (UTi2O6): an integrated study, Mineral. Mag. 84 (2) (Apr. 2020) 313–334, doi:10.1180/mgm.2020.7.
[17] F.A. Charalambous, R. Ram, M.I. Pownceby, J. Tardio, S.K. Bhargava, Chemical and microstructural characterisation studies on natural and heat treated brannerite samples, Miner. Eng. 39 (Dec. 2012) 276–288 no. Supplement C, doi:10.1016/j.mineng.2012.08.006.
[18] D.J. Bailey, M.C. Stennett, N.C. Hyatt, Synthesis and characterization of brannerite compositions for MOX residue disposal, MRS Adv. 2 (10) (Jan. 2017) 557–562, doi:10.1557/adv.2016.631.
[19] E.R. Vance, J.N. Watson, M.L. Carter, R.A. Day, B.D. Begg, Crystal chemistry and stabilization in air of brannerite, UTi2O6, J. Am. Ceram. Soc. 84 (1) (Jan. 2001) 141–144, doi:10.1111/j.1151-2916.2001.tb00621.x.
[20] M. James, J.N. Watson, The synthesis and crystal structure of doped uranium brannerite phases U1−xMxTi2O6 (M=Ca2+, La3+, and Gd3+), J. Solid State Chem. 165 (2) (May 2002) 261–265, doi:10.1006/jssc.2002.9519.
[21] A. Mesbah, et al., Direct synthesis of pure brannerite UTi2O6, J. Nucl. Mater. 515 (Mar. 2019) 401–406, doi:10.1016/j.jnucmat.2019.01.003.
[22] Y. Zhang, L. Kong, I. Karatchevtseva, R.D. Aughterson, D.J. Gregg, G. Triani, Development of brannerite glass-ceramics for the immobilization of actinide-rich radioactive wastes, J. Am. Ceram. Soc. 100 (9) (Sep. 2017) 4341–4351, doi:10.1111/jace.14975.
[23] Y. Zhang, I. Karatchevtseva, L. Kong, T. Wei, Z. Zhang, Structural and spectroscopic investigations on the crystallization of uranium brannerite phases in glass, J. Am. Ceram. Soc. 101 (11) (Nov. 2018) 5219–5228, doi:10.1111/jace.15750.
[24] Y. Zhang, L. Kong, R.D. Aughterson, I. Karatchevtseva, R. Zheng, Phase evolution from Ln2Ti2O7 (Ln=Y and Gd) pyrochlores to brannerites in glass with uranium incorporation, J. Am. Ceram. Soc. 100 (11) (Nov. 2017) 5335–5346, doi:10.1111/jace.15051.
[25] Y. Zhang, T. Wei, Z. Zhang, L. Kong, P. Dayal, D.J. Gregg, Uranium brannerite with Tb(III)/Dy(III) ions: phase formation, structures, and crystallizations in glass, J. Am. Ceram. Soc. 102 (12) (2019) 7699–7709, doi:10.1111/jace.16657.
[26] J. Evans, Advanced input files & parametric quantitative analysis using topas, Mater. Sci. Forum 651 (May 2010) 1–9 10.4028/www.scientific.net/MSF.651.1.
[27] A.A. Coelho, TOPAS and TOPAS-Academic: an optimization program integrating computer algebra and crystallographic objects written in C++, J. Appl. Crystallogr. 51 (1) (Feb. 2018) Art. no. 1, doi:10.1107/S1600576718000183.
[28] A.J. Dent, et al., B18: a core XAS spectroscopy beamline for Diamond, J. Phys. Conf. Ser. 190 (Nov. 2009) 012039, doi:10.1088/1742-6596/190/1/012039.
[29] B. Ravel, M. Newville, ATHENA, ARTEMIS, HEPHAESTUS: data analysis for X-ray absorption spectroscopy using IFEFFIT, J. Synchrotron Radiat. 12 (4) (Jul. 2005) 537–541, doi:10.1107/S0909049505012719.
[30] M.C. Dixon Wilkins, E.R. Maddrell, M.C. Stennett, N.C. Hyatt, Synthesis and characterisation of high ceramic fraction brannerite (UTi $_2$ O $_6$) glass-ceramic composites, IOP Conf. Ser. Mater. Sci. Eng. 818 (Apr. 2020) 012018, doi:10.1088/1757-899X/818/1/012018.
[31] N.C. Hyatt, C.L. Corkhill, M.C. Stennett, R.J. Hand, L.J. Gardner, C.L. Thorpe, The HADES facility for high activity decommissioning engineering & science: part of the UK national nuclear user facility, IOP Conf. Ser. Mater. Sci. Eng. 818 (Apr. 2020) 012022, doi:10.1088/1757-899X/818/1/012022.